© IWA Publishing 2020
1011

Water Practice & Technology Vol 15 No 4
doi: 10.2166/wpt.2020.079

Nano-zeolite-graphene oxide composite for calcium hardness removal: isotherm and kinetic study

Ram Ashok Konale*, Nilesh Keshavrao Mahale and Sopan Tukaram Ingle

School of Environmental and Earth Sciences, Kavayitri Bahinabai Chaudhari North Maharashtra University, Umavi Nagar, Jalgaon, MS 425001, India

*Corresponding author. E-mail: ramkonale@gmail.com

Abstract

The present study is an attempt to synthesize and explore the applications of the synthetic nano-zeolites (nZ) and its composites with graphene oxide (GO) for water purification. The modified Hummer's method and hydrothermal methods were applied for the synthesis of the graphene oxide and nano zeolites respectively, followed by the preparation of the composite with the ultrasonic method. Scanning electron microscopy, energy dispersive analysis of X-rays, Fourier transform infrared spectroscopy and X-ray fluorescence were used for physico-chemical characterization of the composite. The various parameters of adsorbent dose, contact time, initial and final pH of solution were optimized for the removal of calcium hardness. The results indicate optimum removal (98%) can be reached at pH 7 while the removal is highly adsorbent dose-dependent. The nZGO removal data were investigated by pseudo-first-order, pseudo-second-order, Elovich, and intraparticle diffusion. In that, pseudo-second-order and intraparticle diffusion models are best fitted to the experimental data. The experimental data were also analysed by Langmuir, Freundlich and Temkin isotherms, the experimental data follows the Langmuir isotherm and the determination coefficient is 0.99.

Key words: adsorption, calcium hardness, isotherm, nanocomposite

Highlights

- Nano-zeolite-graphene composite synthesized from hazardous fly ash via hydrothermal reaction.
- The crystallographic study of Nano-zeolite with framework is studied in detail.
- The molecular sieve in the composite acts as effective sites for cation exchange.
- The synthesized composite is a highly effective material for water softening.

Graphical Abstract

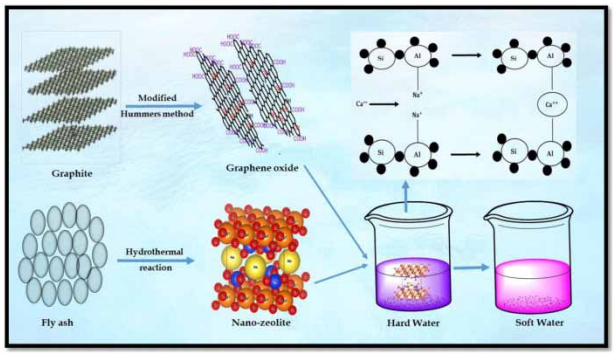

INTRODUCTION

Water quality plays a vital role for its use in industrial, domestic as well as agricultural purposes. Zhi & Zhang (2014) reported interior water quality with respect to chemical contaminants; that is, hardness,

Water Practice & Technology Vol 15 No 4
doi: 10.2166/wpt.2020.079

nitrate, heavy metals and soluble ions, in urban as well as a rural area of the world (Amarasooriya & Kawakami 2019; Ahamad *et al.* 2020). Hardness is a major challenge for groundwater, which is ensured to be the source of water for various purposes. It creates the problem of scaling of boilers, washing machines, and pipes, and difficult lathering for industries. Hard water also creates health problems in human beings. Disorders like urolithiasis, cardiovascular disorders, kidney problems, and even cancer were reported by Rolence (2016). Currently, several techniques have been used to solve the problems such as the deionization process, adsorption, lime soda, nano-filtration (Madarasz *et al.* 2014), microbial and ion exchange processes. The natural zeolites have shown good adsorption properties and are used for purification of water (Gougazeh & Buhl 2013; Madarasz *et al.* 2014).

Graphene is a mono-atomic layer of graphite which is an emerging star on the horizon of material science in the 21st century. Geim & Novoselov (2014) synthesized two-dimensional graphene material for the application of ground-breaking experiments. The unique physicochemical characteristics of graphene oxide; that is, its large surface area (2,600 $m^2\ g^{-1}$), electrical mobility ($em^2v^{-1}s^{-1}$), conductivity (500 $W\ m^{-1}\ K^{-1}$) and mechanical properties have made graphene oxide an ideal adsorbent (Maab *et al.* 2016).

Being a carbon nanomaterial, graphene oxide contains a number of active functional groups like carboxyl, carbonyl, epoxy and hydroxyl which makes graphene a strong candidate for target-specific adsorption (MeiJiao *et al.* 2013). The study by Soltani & Lee (2016) reveals that, due to their high surface area, negative surface charge and highly mobile π-electrons, graphene, graphene oxides, and its composites are efficient adsorbents and are widely used for environmental applications (Kar *et al.* 2016).

Although fly ash has wide applications (Koshy & Singh 2016), mainly about 20% of total fly ash generated from the thermal power plant is used in the cement production (Zhang *et al.* 2011; Izidoro *et al.* 2013). A large quantity of fly ash is dumped in land with resulting harmful effects on the environment (Molina & Poole 2004). Fly ash mostly consists of Al and Si in the form of aluminosilicate, with traces of Fe, Na, K, Ca, Ti and S. It also contains crystalline minerals in minor quantities such as mullites, lime anhydrite and quartz (Soni & Shukla 2018). However, the adsorption efficiency of fly ash is lower in comparison to the commercial adsorbents, consequently (Hong *et al.* 2017), the experiments are being performed with various chemical reactions for the improvement of the fly ash adsorption capacity (He *et al.* 2016).

Zeolites are a significant group of crystalline aluminosilicate crystalline materials and they have generally used in adsorption of contaminants and ion exchange process (Ferrarini *et al.* 2016). It is mainly composed of crystalline solid structures made of silicon, aluminium, and oxygen. Zeolites naturally occur in small quantities only, hence synthetic zeolites are very popular for their catalytic characteristics and other properties like ion exchange and adsorption (Liu *et al.* 2011).

Literature on the removal of hardness from water by zeolite is scarcely available. The present work demonstrates a novel synthesis method for nano-zeolite-graphene oxide (nZGO) composite from fly ash to remove calcium hardness from water (Liu *et al.* 2016; Hailu *et al.* 2019). The natural zeolites have shown good adsorption properties and are used for purification of water, but the limited reserves of zeolite do not permit its application at the commercial level (Gao *et al.* 2011). The fly ash derived nano-zeolite-graphene oxide composite is a better adsorbent for hardness removal from water. The synthesized nZGO composite may also be investigated as a catalytic converter for auto exhausts.

EXPERIMENTAL DETAILS

Materials

Graphite powder, sodium nitrate ($NaNO_3$), sodium hydroxide (NaOH), potassium permanganate ($KMnO_4$), and hydrochloric acid (HCl) were purchased from Fisher Scientific, India. Sulphuric

Water Practice & Technology Vol 15 No 4
doi: 10.2166/wpt.2020.079

acid (H_2SO_4) and hydrogen peroxide (H_2O_2) were supplied by Merck. All reagents were used without any further purification.

Preparation of graphene oxide (GO)

GO was synthesized using the modified Hummer's method. For this, concentrated sulphuric acid (H_2SO_4) 69 ml, 3 gram of graphite powder and $NaNO_3$ (1.5 gram) were added in the round bottom flask at less than 5 °C for 20 minutes with continuous stirring. Then subsequently 9 gram of potassium permanganate ($KMnO_4$) was added slowly for 1 hour. The reaction was stirred for 7 hours at 35 °C. After 7 hours, 9 gram of potassium permanganate was added slowly for 15 minutes and the reaction was stirred for 12 hours at room temperature. The gradually brown color was developed which indicates the complete oxidation of graphite (Marcano *et al.* 2010; Zamani & Tabrizi 2016). The reaction mixture was cooled at room temperature and transferred into an ice bath with the addition of 300 ml distilled water. Finally, the brown suspension was further treated with 10 ml hydrogen peroxide (H_2O_2) to reduce residual oxidant, the brown suspension turns to pale yellow. This suspension was highly acidic (pH <4). The mixture was repeatedly washed with dilute ammonium hydroxide solution followed by distilled water until the mixture attained pH 7. The final yield was 5.1 g dried solids after drying in the oven at 60 °C. The mother liquor was analyzed on the atomic absorption spectrophotometer, to ensure that the graphite oxide was free of sodium, potassium and manganese; the solution was free of the trio.

Synthesis of nano-zeolites (nZ)

The fly ash <120 μm particle size was obtained by sieving for the synthesis of nano-zeolite. The dissolved iron oxides were removed by washing the fly ash with 10% HCl for 12 hours. Pre-treated 15 gram of dry fly ash was mixed in 50 ml 8 N NaOH in a Teflon-lined autoclave reactor. The hydrothermal reaction was carried out at 130 °C for 3 hours. The autoclave reactor was cooled until it reached room temperature, and the mixture was washed with distilled water up to pH 7 and dried in the oven at 80 °C for 3 hours (Chen & Lu *et al.* 2018; Zhao *et al.* 2018).

Preparation of nano-zeolite-graphene-oxides composite (nZGO)

250 mg of graphene oxide was mixed in 50 ml of distilled water for ultra-sonic exfoliation for 3 hours. Subsequently, 5 gram of nano-zeolite was added to the exfoliated graphene oxide solution and stirred for 6 hours. The solution of the reaction was filtered and washed several times with distilled water. The reaction mixture of the reaction was dried in the oven at 60 °C for 3 hours. To ensure composite formation, the process was undertaken three times.

Physico-chemical characterization

Investigate the functional groups, Fourier Transformation Infrared spectroscopy (FTIR) (Shimadzu IR Affinity-1) with intensity from 400 to 4,000 cm^{-1} was applied. The crystallographic study was done on an X-ray diffractometer (LabX XRD-6100) with monochromatized Cu-Ka ($\lambda = 0.154056$ nm) radiation at 36 kV, 20 mA samples were scanned in the range of 5–80° with continuous scanning mode and scanning rate was set at 2°/min. The morphological characteristics of the sample were investigated using Field Emission Scanning Electron Microscopy (Hitachi FESEM S-4800) with voltage accelerated voltage at 20 keV. The composition of the elements of the samples were studied using Energy dispersive analysis of X-rays (EDX, Bruker Nano). The chemical composition of fly ash was carried

Water Practice & Technology Vol 15 No 4
doi: 10.2166/wpt.2020.079

out with the help of an X-ray fluorescence spectroscope with glass tablets FLX-SP1, Voltage/kV: 38.0, Current/μA: 15.0 for MCA peak calibration (ED-XRF SPECTRO XEPOS III).

Batch adsorption study

In order to find the batch adsorption behaviour of calcium hardness onto nZGO, the experiments were performed at room temperature. The standard stock solution of calcium hardness was made by dissolving 3.6 gm of calcium chloride in 1,000 ml DI water at neutral pH. The working solution of the required concentration was prepared by serial dilution of the stock calcium hardness solution. For the evaluation of the hardness removal, different amounts of nZGO (250–1,000 mg/L) were mixed into 100 ml calcium hardness solution of known concentration (250–1,000 mg/L) and the mixture was stirred using an orbital shaker at 110 rpm for different time intervals. Subsequently, the supernatant was separated from the mixture by filtration, and the residual calcium hardness was determined by titration with the EDTA method.

The pH optimization was performed with the nZGO (250 mg/L) at different pH (1–14). The pH of the solution was attuned using 0.1 N HCl/NaOH before the addition of nZGO. For dose on optimization, different amounts of adsorbents (250–1,000 mg/L) were used and an optimum adsorbent dose of 1,000 mg/L at 110 rpm stirring speed was observed. All the experiments were performed three times and the mean was considered as a final value.

RESULT AND DISCUSSION

Chemical composition of fly ash

The XRF results reveal the chemical composition of the fly ash used for the preparation of nZ. The major constituents were silica (76.68%), aluminium (17.33%), calcium (1.6%) and titanium dioxides (1.42%) with other elements in trace quantity. The loss on ignition was found to be 47.52%. Table 1 also shows the chemical composition of major and minor elements obtained by XRF analysis. In general, results are similar for most of the elements.

FTIR

Figure 1 shows the FTIR spectra of GO synthesised by the modified Hummer's method. The FTIR spectrum of GO shows strong and broad O-H stretching vibration band at 3,630 cm^{-1}, 3,439 cm^{-1}, -OH from (H_2O) at 3,190 cm^{-1}, at 2,824 cm^{-1} for –OH of carboxylic group, carboxyl C = O stretching band at 1,737 cm^{-1}, aromatic C = C at 1,574 cm^{-1} C-O-H deformation band at 1,386 cm^{-1}, 1,196 – OH (Phenolic), C-C skeletal stretching vibration at 1,053 cm^{-1}, and C-O skeletal stretching band can be seen at 968 cm^{-1}, 828 cm^{-1} and 698 cm^{-1}.

The FTIR spectra in Figure 2 of nano zeolite are helpful for the identification of bands related to the construction of the aluminosilicate framework of zeolites. The asymmetric stretching vibrations bridge bonds of Si-O-Al are assigned to the band at 1,006 cm^{-1} and around 670 cm^{-1} is symmetric stretching vibrations of bridge bonds (Mozgawa 2001). The characteristic single band of zeolite around 1,006 cm^{-1} has resulted in a hydrothermal reaction of fly ash with NaOH. The bands at the wave number 489 cm^{-1} are the characteristic bending vibration of oxygen hexagonal rings present in zeolites.

The FTIR spectra in Figure 3 depict the bands of the nZGO. In this spectrum, the nano zeolite crystal framework dominates, whereas the O-H of the graphene oxide is reduced to a considerable extent and the band for the hydroxyl stretching vibration at 3,439 cm^{-1} is hardly visible. The other bands of GO are observed as at 1,737 cm^{-1} (C = O), 1,386 cm^{-1} (-C-OH), and (-C-C-) 1,053 cm^{-1} (Xia &

Water Practice & Technology Vol 15 No 4
doi: 10.2166/wpt.2020.079

Table 1 | Chemical composition of major and minor elements in fly ash

Sr. No.	Element	Concentration	Unit
1	Silicon dioxide (SiO_2)	71.04	%
2	Aluminium oxide (Al_2O_3)	17.33	%
3	Potassium (K_2O)	0.959	%
4	Calcium oxide (CaO)	1.65	%
5	Titanium dioxide (TiO_2)	1.42	%
5	Magnesium oxide (MgO)	0.43	%
7	Phosphorus pentoxide (P_2O_5)	0.15	%
8	Manganese oxide (MnO)	0.06	%
9	Ferric oxide (Fe_2O_3)	5.58	%
10	Bismuth (Bi)	0.132	%
11	Barium (Ba)	0.05	%
12	Chlorine (Cl)	0.03	%
13	Zirconium (Zr)	0.03	%
14	Strontium (Sr)	0.01	%
15	Zinc (Zn)	0.01	%
16	Cerium (Ce)	0.008	%
17	Copper (Cu)	0.007	%
18	Vanadium (V)	0.006	%
19	Chromium (Cr)	0.005	%
20	Yttrium (Y)	0.005	%
21	Nickel (Ni)	0.005	%
22	Rubidium	48.8	%
23	Lanthanum (La)	0.004	%
24	Lead (Pb)	0.004	%
25	Other element	1.075	%

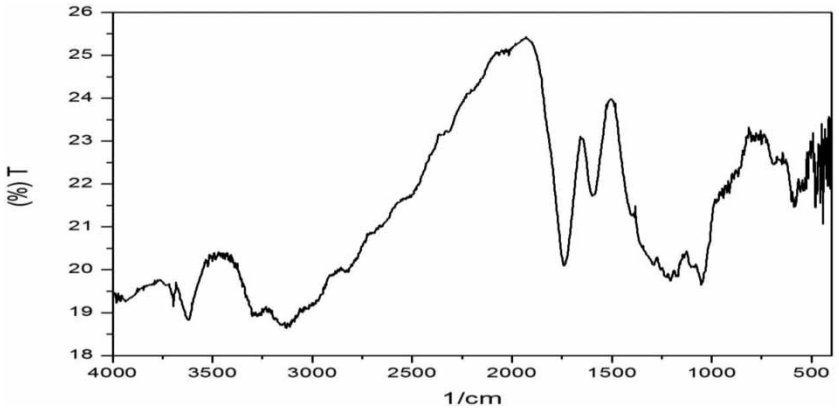

Figure 1 | FTIR spectrum of graphene oxide.

Gerson 2018). The asymmetric stretching vibration of bridge bonds in nano zeolite for Si-O-Al is also present around 1,016 cm^{-1} with symmetric stretching vibration at 670 cm^{-1} (Agarwal & Rani 2018). All these observations validate the formation of the nano-zeolite-graphene oxide composite. The reduction of the hydroxyl group in the nZGO indicates the reducing nature of the nano zeolites; for further clarity, a detailed experimental study is necessary (Jha & Singh 2018).

Water Practice & Technology Vol 15 No 4
doi: 10.2166/wpt.2020.079

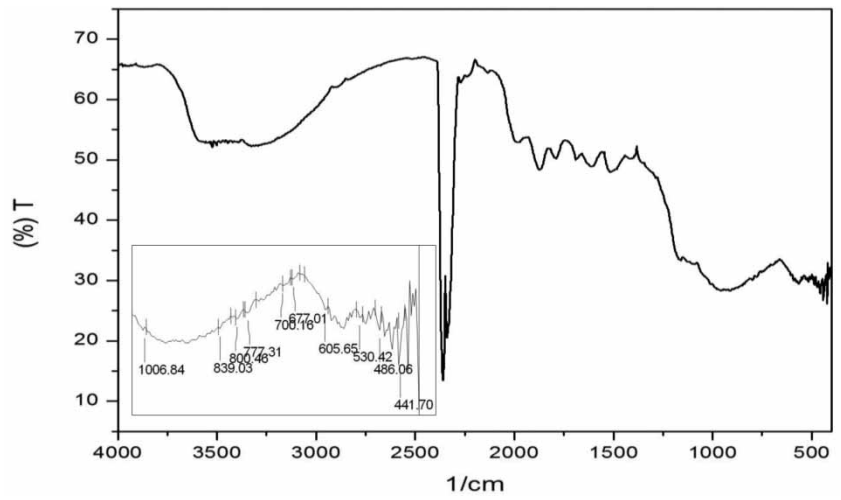

Figure 2 | FTIR spectra of nano-zeolites.

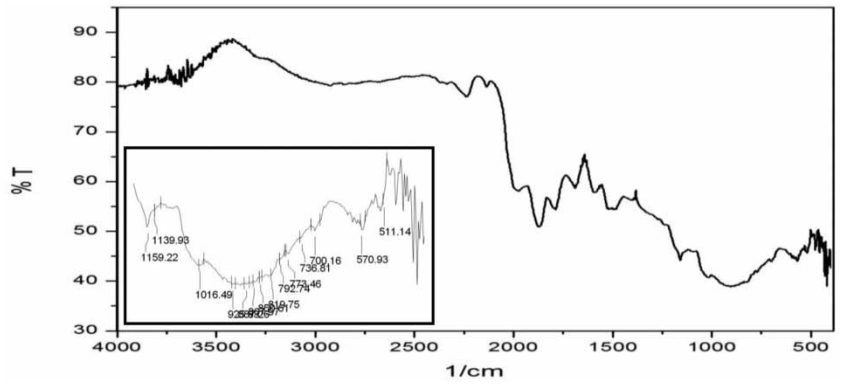

Figure 3 | FTIR spectra of nZGO composite.

Crystallographic properties

The XRD patterns of the solid products of GO, nZ, and nZGO composite are shown in Figure 4. The XRD pattern of graphene oxide shows diffraction peaks at 12.5° and 43.2°. The values of the diffraction peaks are in good agreement with the previously reported literature (Gebhardt *et al.* 2014). The peak intensity at 25.97° in the nZGO composite is reduced considerably in comparison to pristine GO. After the Reitveld refinement in PANalytical High ScorePlus V. 30, search and match of peaks revealed the structure of the nano zeolite as almost similar to wonesite. The crystal structure was formed with the help of the data processing software VESTA (Figure 4(b). The lattice type was C with the symmetry C2/m, the unit cell dimensions were found to be $a = 6.00$, $b = 10.60$, $c = 9.6$ Å, $\alpha = 90$, $\beta = 104.100$, $\gamma = 90°$ and the unit cell volume was 592.16 Å3. From Figure 4(b) it is clear that the hexagonal oxygen ring formation is present in the structure. The synthesized nano zeolite shows a triclinic structure in which the two tetrahedral sheets are set apart through the interlayer region. The interlayer region is partially occupied by sodium ions (Kogure *et al.* 2005).

Morphological properties

The surface characteristics of graphene oxide were studied using FESEM. The graphene oxide shows a layered and three-dimensional nature (Figure 5(a)), thick edges of graphite have exfoliated after

Water Practice & Technology Vol 15 No 4
doi: 10.2166/wpt.2020.079

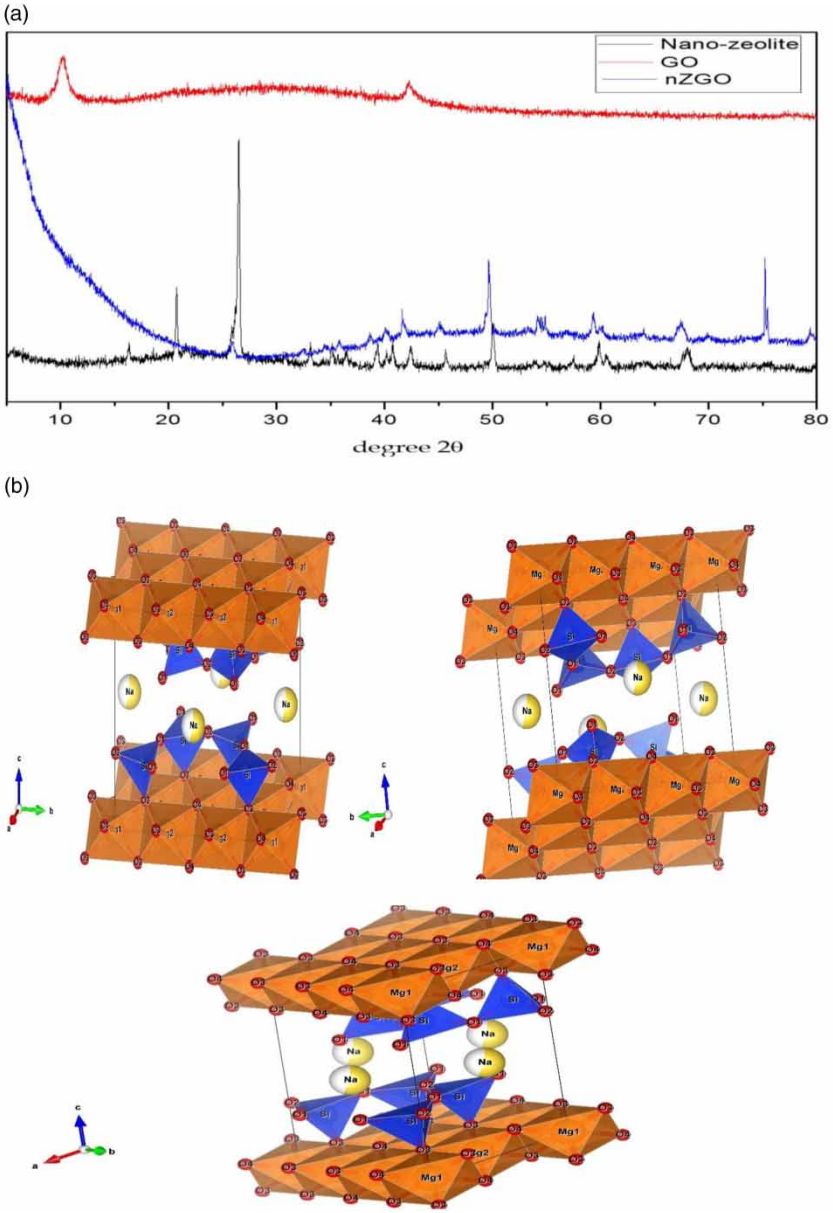

Figure 4 | (a) X-ray diffraction pattern of nZGO, nZ and GO. (b) Three dimensional crystal structure of nZGO composite.

oxidation. The image shows the multilayer graphene oxide sheet as well as folding at the edges. Energy dispersion X-ray analysis was carried out for estimation of the elemental composition (carbon and oxygen) in the sample. The increased oxygen content in GO can be seen in the inset table of Figure 5(b).

FESEM images of fly ash show the irregular spheroidal crystal morphology, it has spherical particles with smooth surfaces and edges (Figure 5(c)). The spheroidal fly ash particles were transformed into smooth edged-irregular elliptical and spherical shaped nano-zeolites (Figure 5(e)). This shape and size transformation provides a large surface area with highly active sites (Figure 5(j) and 5(k)).

The rough surface of the nZ adsorbent resulted in a comparatively increased surface area compared to fly ash. The average diameter of the nZ was found to be approximately 20 nm. The size of the fly ash particles size reduces significantly after hydrothermal reaction with sodium hydroxide and forms nano zeolites. The EDX results (Figure 3(f)) indicates the replacement of aluminium by sodium in the fly ash. Figure 3(f) also indicates the elemental presence of Na, Al, Si and O in nZ.

Water Practice & Technology Vol 15 No 4
doi: 10.2166/wpt.2020.079

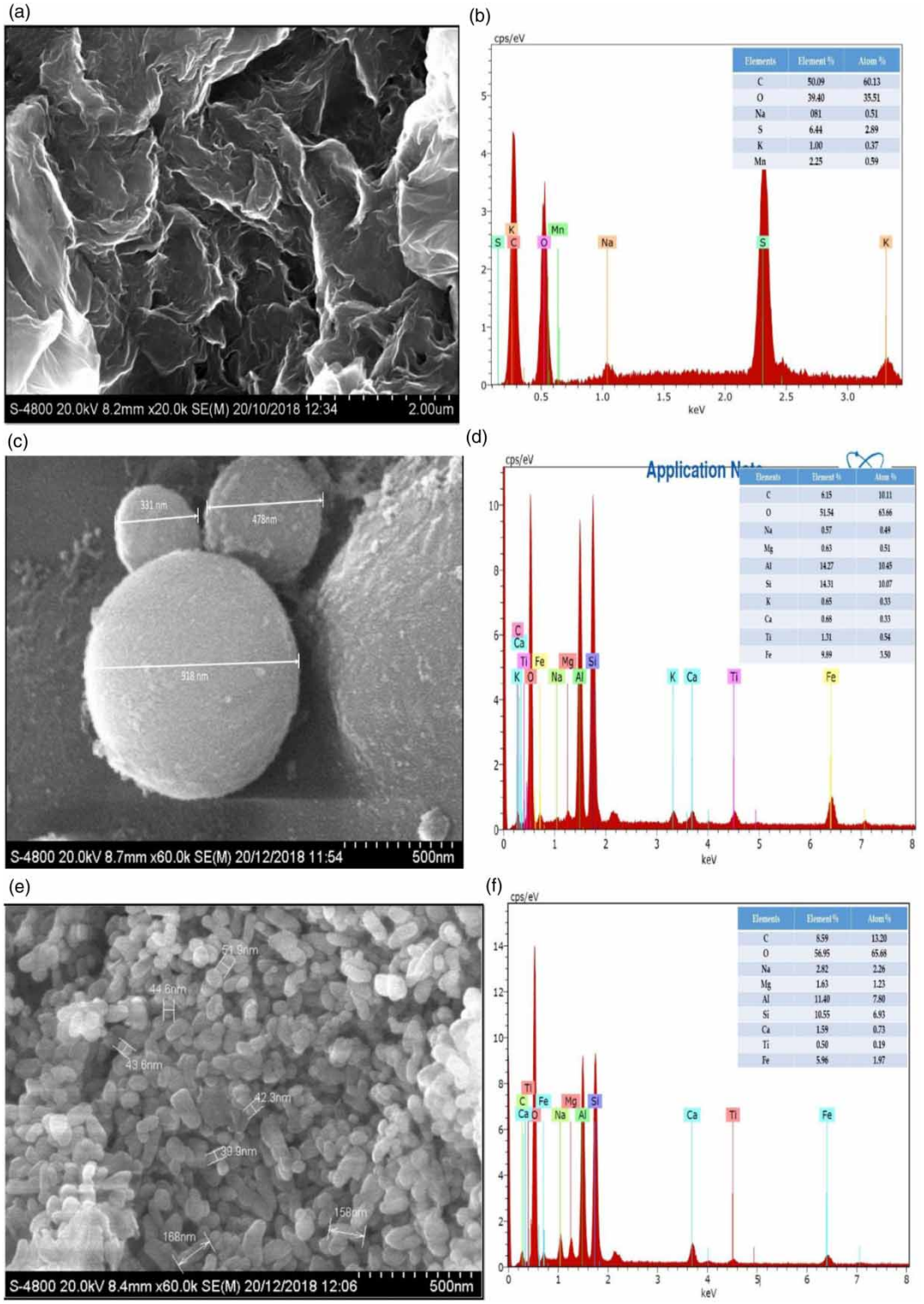

Figure 5 | SEM images showing the different morphologies of GO (a), fly ash (c), nZ (e) and nZGO (g) and the EDX graph of elemental composition GO (b), fly ash (d), nZ (f) and nZGO (h), three-dimensional profiles of roughness images of FA (i), nZ (j) and nZGO (k). *(continued)*.

FESEM observation of nZGO shows that the nano zeolites are uniformly coated with GO sheets as a result of pressure and temperature during the hydrothermal reaction. The bright crystals of the nZ turned black in color after the hydrothermal treatment. The composite formation is evidenced by the color change as well as the EDX analysis results (Figure 5(h)). The GO sheets with hydrophilic

Water Practice & Technology Vol 15 No 4
doi: 10.2166/wpt.2020.079

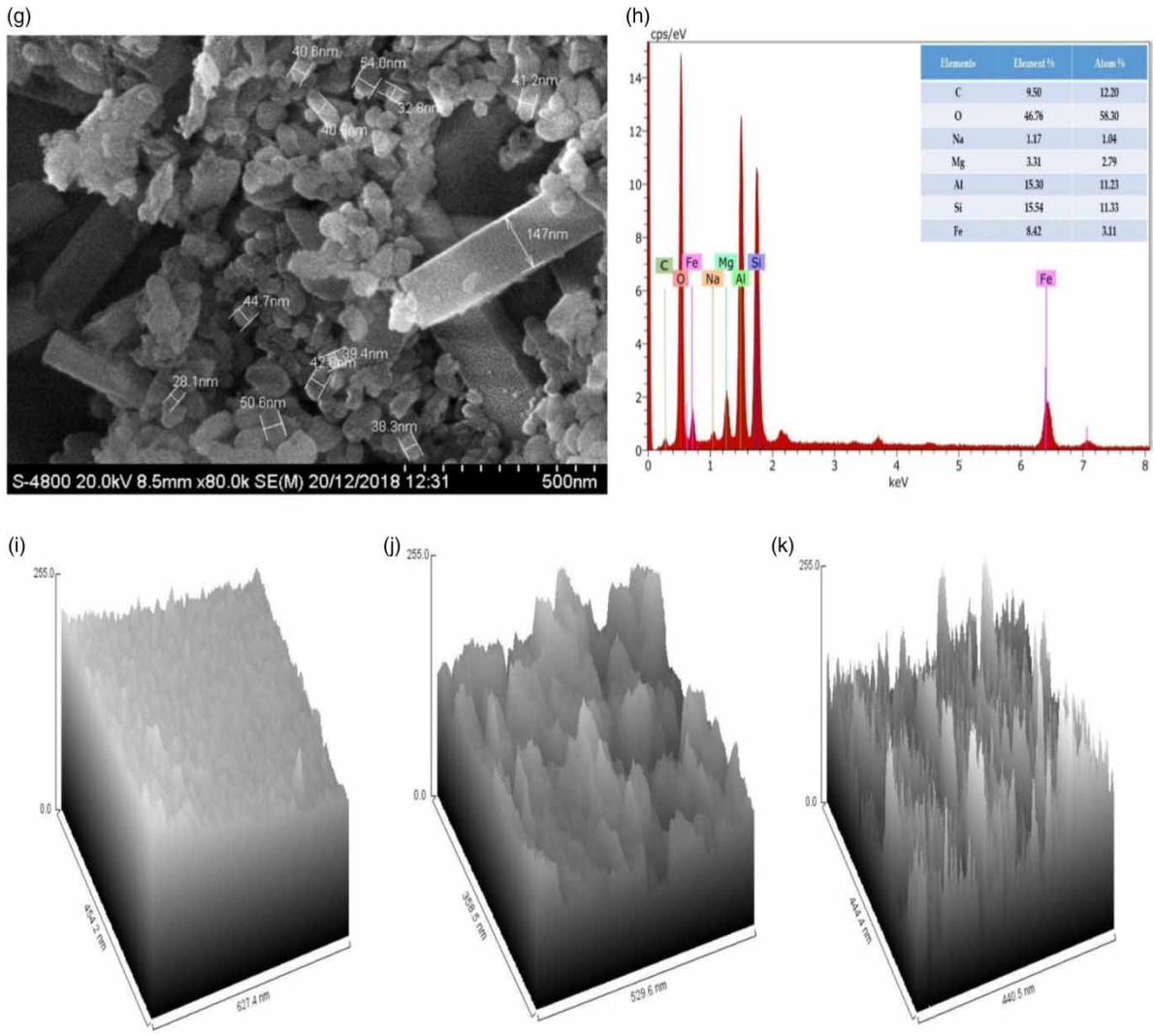

Figure 5 | Continued.

nature have favourable interaction with nano zeolite crystals. Figure 6(a) is the histogram of the nZ particles size, it reveals the particles ranged between 10 and 130 nm; however, the particle size 10–40 nm is of maximum frequency. In Figure 6(b), the histogram of the nZGO particle can be seen with a size distribution between 10–140 nm; the particle size of 10–30 is dominated by high frequency.

pH effect on adsorption

The pH of the calcium hardness solution is a significant influence on the adsorption process, which is directly affected by the functional groups present on the adsorbent surface by changing the charge of the adsorbent surface.

The experiments on the effect of pH on the adsorption process were performed at pH 1–14 with the 250 mg/L calcium hardness solution concentration; contact time was 2 hours at 27 °C and adsorbent concentration 250 mg/L. The results are shown in Figure 7; adsorption is about 40% at pH 1–6 and adsorption also decreased in the pH range of 8–14. The neutral pH condition is favourable for maximum adsorption of calcium hardness by nZGO with 98% achieved. Acidic and basic conditions of the solution hamper the adsorption mechanism (Singh & George 2018)

$$(\Delta\,\mathrm{pH}) = \frac{(\mathrm{pH\ \ Initial\ \ - pH\ \ Final})}{\mathrm{pH\ \ Initial}} \tag{1}$$

Water Practice & Technology Vol 15 No 4
doi: 10.2166/wpt.2020.079

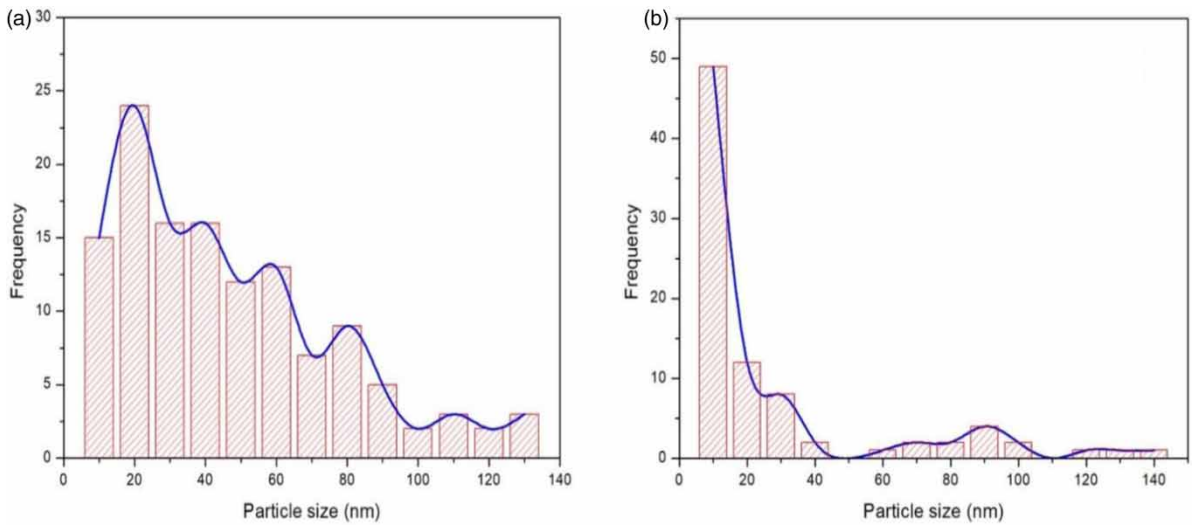

Figure 6 | Particle size distribution of nZ (a) and nZGO (b).

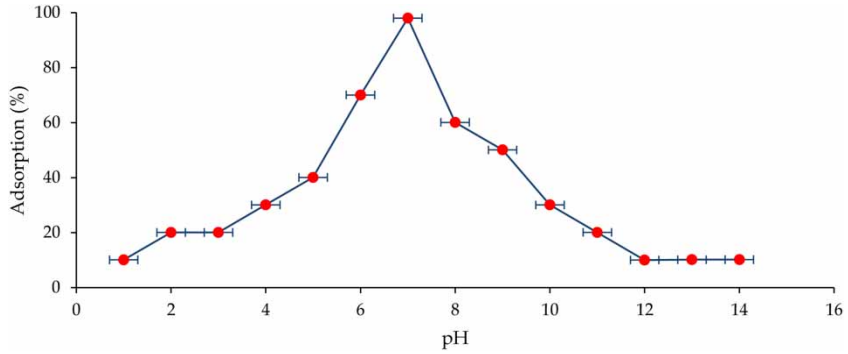

Figure 7 | pH effect on calcium hardness adsorption by nZGO, adsorbent dose 250 mg/L and calcium hardness concentration 250 mg/L at 27 °C.

where Δ pH is the charge on the adsorbent surface, which is equal to zero, the initial pH of the solution is the pH before treatment, whereas pH final is the pH of the solution after treatment. The resultant zero-point charge of the composite adsorbent was found at pH 7, this indicates the nZGO composite surface has a positive charge in acidic conditions while the surface has a negative charge under basic conditions. The influence of pH on the nZGO is shown in Figure 8. The optimum equilibrium adsorption capacity of hardness was observed at pH 6 to 8. The results indicate, though the adsorption efficiency is highly favourable at neutral pH, hardness removal up to the accepted limits can be achieved in the pH range of 6–8 (Barathi *et al.* 2014).

Effect of contact time

The R for adsorption efficiency and q for capacity of adsorption were calculated using the following equation:

$$R = \frac{(C_0 - C_l)}{C_0} * 100\% \tag{2}$$

$$q_t = \frac{(C_0 - C_l)m}{V} \tag{3}$$

Water Practice & Technology Vol 15 No 4
doi: 10.2166/wpt.2020.079

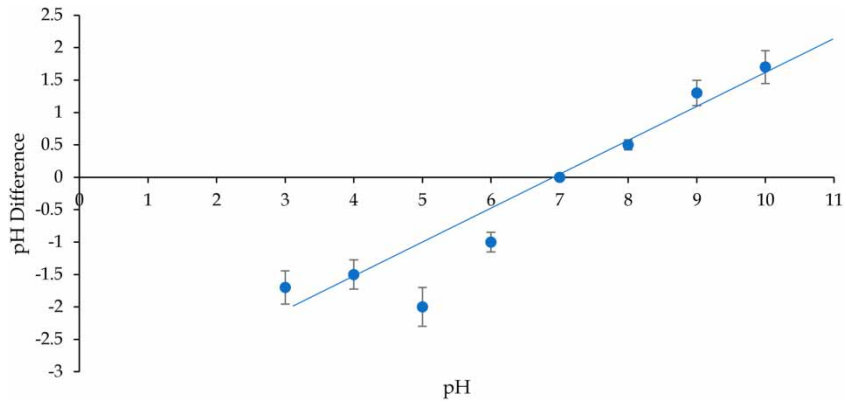

Figure 8 | Zero point charge.

where C_0 (mg/L) is the initial calcium hardness, C_l is the residual concentration of calcium ions, V (litres) is solution volume and m (mg) is the adsorbent mass.

The effect of contact time was studied at room temperature and with intervals of 15–300 minutes. Figure 9 shows the relationship between adsorbent adsorption time and calcium absorption efficiency. It was revealed that calcium removal is rapid for 15–120 minutes and thereafter removal capacity is at a slower rate. The percentage of calcium hardness removal comes to equilibrium within 120 minutes. Further increase in contact time did not show significant change in hardness removal. This may explore the adsorption on the outer part of the adsorbent surface (Geethamani *et al.* 2013).

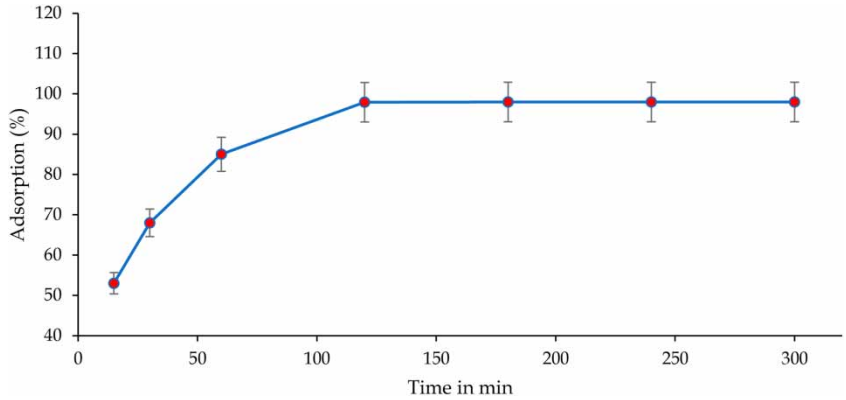

Figure 9 | Calcium hardness adsorption (%) vs. contact time, adsorbent dose 250 mg/L, calcium hardness concentration 250 mg/L at pH 7.

Effect of initial calcium hardness concentration

The effect of initial calcium hardness concentration in the water solution was studied to find the adsorption capacity of nZGO. The experiments were conducted at pH 7 for 120 minutes (Figure 10) duration with four different adsorbent doses (250, 500, 750 and 1,000 mg/L) for four different calcium hardness concentrations, viz. 250, 500, 750, and 1,000 mg/L being used to examine efficiency. It can be observed in Figure 7 that the adsorption capacity declines in both acidic and basic conditions, and the decrease in adsorption capacity may be a result of saturation of the active binding sites on nZGO. The increased dose increases the adsorption up to 1,000 mg/L. With increasing adsorbent dose from 250 to 1,000 mg/L, the adsorption of calcium ions increased from 69 to 98%, respectively. An increase of adsorption of calcium ions with increasing adsorbent dose may be due to the availability of more binding sites for adsorption.

Water Practice & Technology Vol 15 No 4
doi: 10.2166/wpt.2020.079

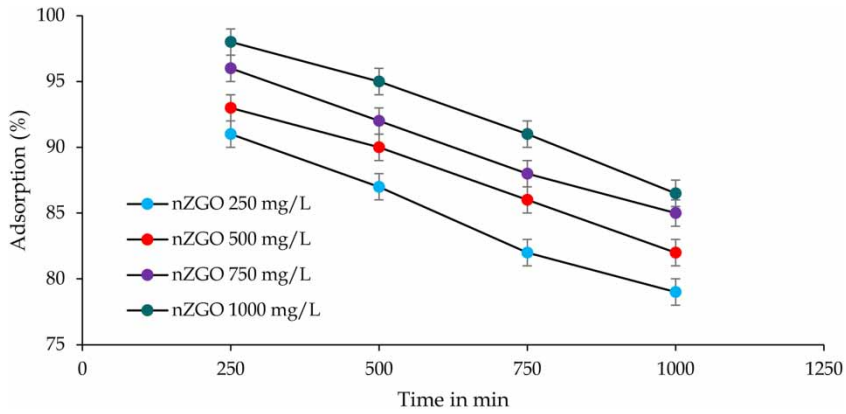

Figure 10 | Variation of calcium hardness adsorption (%) at different adsorbent doses (250–1,000 mg/L), pH 7.

Kinetic study

The various parameters of adsorption kinetics are necessary for determining the adsorption rate, with substantial information for modelling and designing the adsorption mechanism (Jayarathna *et al.* 2015). The kinetics of calcium hardness by nZGO absorption were studied using the pseudo-first-order, pseudo-second-order (Figure 11) and intraparticle diffusion models (Figure 12). Table 3 illustrates the various parameters and correlation coefficients (R^2 values near 1) values. For the conformity, the predicted values of model and experimental data were expressed by the correlation coefficient. The kinetics equations are given below:

Pseudo-first-order equation:

$$log\ (q_e - q_t) = log\ q_e - (K_f/2.303)t \tag{4}$$

Pseudo-second-order equation:

$$t/qt = 1/K_S q_e^2 + \left(\frac{1}{q_e}\right)t \tag{5}$$

where q_e is the equilibrium adsorption capacity (mg/g), q_t is the amount of calcium hardness adsorbed (mg/g) and time t, K_f is the pseudo-first-order rate constant and K_S is the rate constant of the pseudo-

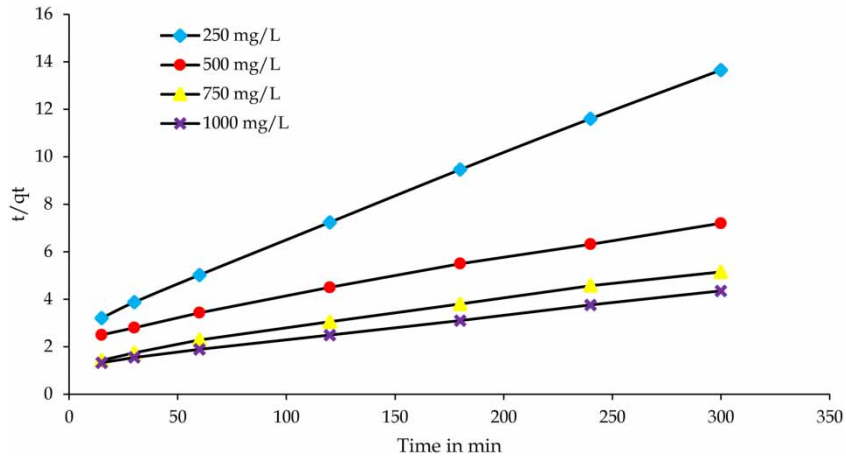

Figure 11 | Pseudo-second-order kinetics of calcium hardness adsorption by nZGO at pH 7.

Water Practice & Technology Vol 15 No 4
doi: 10.2166/wpt.2020.079

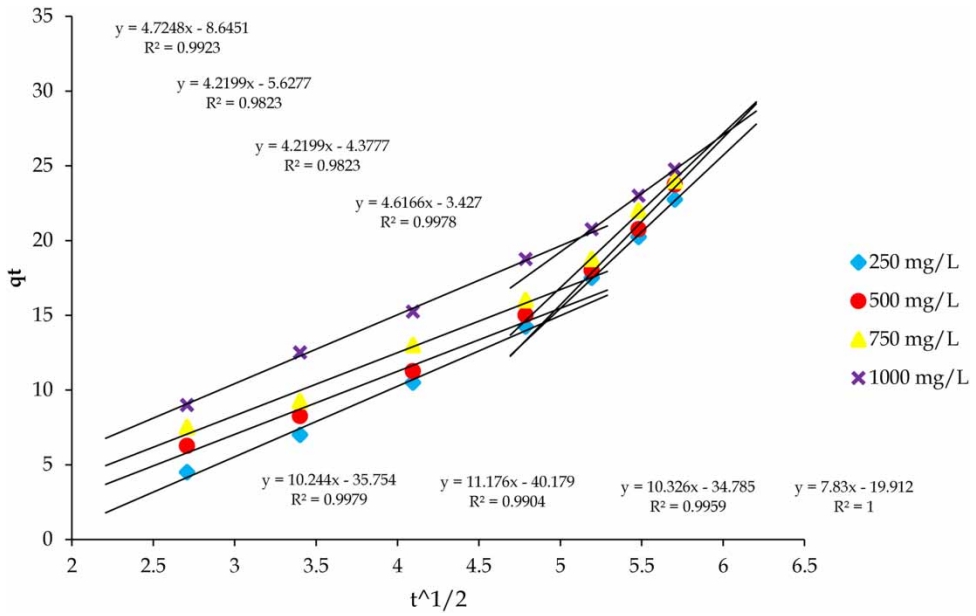

Figure 12 | Intra particle diffusion of calcium ion adsorption by nZGO at different nZGO doses; at pH 7.

Table 2 | Kinetics coefficient values (R^2) of different initial calcium hardness concentrations (250–1,000 mg/L) at pH 7

		Calcium hardness concentration (mg/L)			
Models	**Parameters**	**250**	**500**	**750**	**1,000**
Pseudo-first-order kinetics	$K_f \times 10^2$	0.852	0.230	0.230	0.040
	qe	3.980	10.97	14.79	17.54
	R^2	0.879	0.758	0.856	0.945
Pseudo-second- order kinetics	$K_s \times 10^2$	0.0366	0.016	0.013	0.010
	q_e	2.781	2.379	1.393	1.222
	R^2	0.999	0.995	0.993	0.999
Intra-particle diffusion	$K_{id}1$	4.724	2.453	3.906	3.803
	C	8.645	1.704	3.729	3.800
	R^2	0.992	0.998	0.955	0.998
	$K_{id}2$	10.24	3.842	3.412	3.845
	C	35.75	21.54	3.909	7.251
	R^2	0.997	0.992	0.8844	0.999
Elovich	α	208	2.016	1.966	2.809
	β	0.166	0.084	0.064	0.062
	R^2	0.9791	0.9311	0.9872	0.972

Table 3 | Adsorption equilibrium constants obtained from different isotherms fitting for adsorption of calcium ions

			Adsorbent dose (mg/L)			
Isotherm	**Linear form**	**Parameters**	**250**	**500**	**750**	**1,000**
Langmuir	$C_e/q_e = C_e\alpha_L/K_L + 1/K_L$	q_m (mg/g)	217.3	100	68.49	46.95
		K_L (L/mg)	2.287	2.298	2.329	3.772
		R^2	0.950	0.981	0.999	0.993
Freundlich	$\ln Qe = 1/n\ 1nCe + \ln k_f$	n	1.9775	2.184	2.159	3.063
		K_f (L/mg)	10.40	8.0196	6.2332	9.234
		R^2	0.941	0.972	0.938	0.967
Temkin isotherm	$q_e = B_1\ In\ KT + B_1\ InsC_e$	B1	0.011	0.0211	0.031	0.0403
		KT (L/mg)	1.692	4.421	1.136	4.056
		R^2	0.966	0.967	0.969	0.971

Water Practice & Technology Vol 15 No 4
doi: 10.2166/wpt.2020.079

second-order kinetics (mg/min) (Jethave *et al.* 2017). Figure 11 shows the values of q_e and K_f determined by slope and intercept by plotting log $(q_e - q_t)$ vs. t. In order to find the suitability of the models, four initial hardness concentrations of 250, 500, 750 and 1,000 mg/L were prepared. Table 2 shows the calculated parameters, based on the correlation coefficient value of $R^2 = 0.999$; it can be concluded that the calcium hardness adsorption on the nZGO follows the pseudo-second-order kinetics model; further, this model can be used for the investigation of the adsorption process (Mondal *et al.* 2016).

Despite the high correlation coefficient values for adsorption on the nZGO surface, the second-order kinetic process cannot be pointed out. The above models were not able to distinguish the intra-particle diffusion mechanism. Hence, the intra-particle mass transfer diffusion model was used to determine the rate control step. The kinetic adsorption process expressed in Equation (6) is another alternative method.

$$q_t = K_{id}\, t^{1/2} + C \tag{6}$$

where q_t is the number of calcium ions adsorbed by nZGO at time t, k is the intraparticle diffusion constant (mg/g·min$^{0.5}$) and C is the intercept. The intraparticle diffusion model was proposed by Weber & Morris (1963) (Senusi & Karim 2011; Geethamani *et al.* 2013). This can be calculated by the plot of q_t vs. t is based on the intraparticle diffusion model, which is a straight line if the adsorption mechanism expresses the only intraparticle diffusion process (Jethave *et al.* 2017). In Table 2 are shown the obtained rate constants of intraparticle diffusion. For the intraparticle diffusion model fitting for 250–1,000 mg/L calcium hardness concentration and adsorbent dose of 250 mg/L, each set of experimental results shows that two different slopes are fitted with different straight lines (Figure 12). This model shows the multi-linear fitting of the experimental data of the adsorption process involves more than one kinetic mechanism and more than two steps influenced the adsorption process. The experimental data in this model explained that the adsorption process of calcium ions by nZGO involves more than one kinetic mechanism.

The Elovich equation was applied to evaluate the kinetics of chemisorption of calcium ions by nZGO it depends on the adsorption capacity in linear form and is obtained from Equation (7).

$$qt = \left(\frac{1}{\beta In(\alpha\beta)} + \frac{1}{\beta}\right) In\ t \tag{7}$$

where q is the amount of calcium ions adsorbed at time t, α is the desorption constant and β represents the initial adsorption rate. The plot of q_t versus $ln(t)$ should yield a linear relationship with a slope and intercept of $(1/\beta)$ and $(1/\beta)\ ln\ (\alpha\beta)$, respectively. The Elovich constants, taken from the intercept of the conventional line and slope, are shown in Table 2 (Ghaedi *et al.* 2015).

The kinetics study shows that the nZGO obeys the pseudo-second order kinetics and also satisfies the Elovich equation.

Isotherm adsorption analysis

The adsorption isotherm study of the adsorption process for water purification is an important step. The adsorption isotherm models were used to investigate the interaction between calcium ions and adsorbent; that is, nZGO. As per Langmuir (1918), q_e is the amount of adsorbate; that is, Ca^{++} ions adsorbed per unit weight of adsorbent (nZGO) and C_e is the equilibrium concentration of adsorbate solution (mg/L), at constant temperature; this is the adsorption isotherm (Jethave *et al.* 2017). The experimental values of adsorption are tested with Langmuir, Freundlich and Temkin isotherm models. The linearized forms of the equations predict adsorbent-adsorbate behaviour.

Water Practice & Technology Vol 15 No 4
doi: 10.2166/wpt.2020.079

The equilibrium of the adsorption process was described by fitting the experimental data with Langmuir, Freundlich and Temkin models, which are used to represent the equilibrium adsorption isotherm. The Langmuir isotherm model approved that superlative adsorption appears when an nZGO adsorbent surface consists of a saturated monolayer of solute molecules. It further assumes that the energy of adsorption is the same and there is no movement of adsorbates on the surface. Instead, the Freundlich isotherm model describes the adsorption of calcium ions from a liquid to a heterogeneous solid surface adsorbent (nZGO). The results obtained are presented in Table 3.

$$\frac{Ce}{qe} = \frac{Ce\alpha_L}{K_l} + \frac{1}{K_L} \tag{8}$$

where $q_m = \alpha L/K_L$ (mg/g) is the monolayer adsorption capacity of the adsorbent, K_L (L/mg) Langmuir isotherm constant, q_e solid-phase adsorbate equilibrium concentration and C_e represent equilibrium concentration. A plot of C_e/q_e versus C_e gives a straight line where slope is $\alpha L/K_L$ and intercept equal to $1/K_L$. The correlation coefficient values between (R^2 0.950–0.993) confirms the adsorption process followed the Langmuir isotherm model. The van der Waals forces lead aggregation between the heterogeneous surface of the adsorbent and adsorbate with monolayer adsorption. The results reveal that the surface of the adsorbent has vast amounts of active sites for calcium ion adsorption. The q_{max} value obtained from the Langmuir isotherm (Figure 13) was found to be 217 mg/g, which is close to the experimental values of 227 mg/g.

$$InQe = \frac{1}{InCe} + Ink_f \tag{9}$$

The Freundlich isotherm model is usually applied when the adsorption sites are not identical and there is multilayer adsorption. Where k_f is the Freundlich constant and n is a heterogeneity adsorbent surface. The Freundlich isotherm constant values were calculated using the slope and intercept of the linear plot Inq_e versus Inc_e, while the values between R^2 (0.941–0.967) are shown in Table 3, though the experimental values display a linear nature but the confidence interval is lower in comparison to the Langmuir isotherm (Araghia & Entezari 2015; Nigri *et al.* 2017).

$$q_e = B_1 In\ KT + B_1\ InsC_e \tag{10}$$

The Temkin isotherm model anticipates that the adsorption of the heat of all molecules should decrease linearly with increasing adsorbate overlapping on the adsorbent (i.e. nZGO) surface, and adsorption of adsorbate (calcium ions) is characterized by uniform distribution with maximum binding energy (Kadir & Ismail 2017; Petriciolet *et al.* 2017). The Temkin isotherm equation is given as Equation

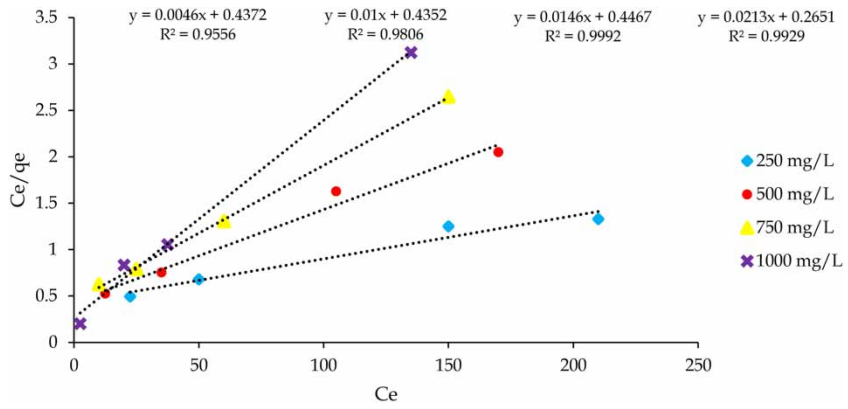

Figure 13 | Langmuir isotherm model for calcium hardness removal at four different adsorbent doses (250–1,000 mg/L).

Water Practice & Technology Vol 15 No 4
doi: 10.2166/wpt.2020.079

(10). Where KT is the equilibrium binding constant (mg/L), T is the absolute temperature in K, and B_1 is for the heat of adsorption. The constants calculated from the Temkin isotherm are shown in Table 3. The heat of adsorption (B_1) value should decrease with increase in adsorbent dosage but the increasing values of (B_1) indicates the Temkin isotherm model is not in agreement with the experimental data.

Separation factor

In order to find the feasibility of the adsorption process, the dimensional separation factor R_L is calculated using the Langmuir constant (Fegade *et al.* 2018).

$$R = \left(\frac{1}{1 + \alpha_L C_o}\right) \tag{11}$$

If $R_L > 1$ unfavourable, $0 < R_L < 1$ favourable, $R_L = 0$ irreversible and $R_L = 1$ linear.
Where C_0 is the calcium ion initial concentration (mg/L), R_L represents the condition for adsorption and αL is the Langmuir constant (L/mg). The calculated values in the present study for R_L were found to be between 0.186 and 0.012, which indicates the favourable condition for calcium ion adsorption onto nZGO surface (Figure 14) (Geethamani *et al.* 2013).

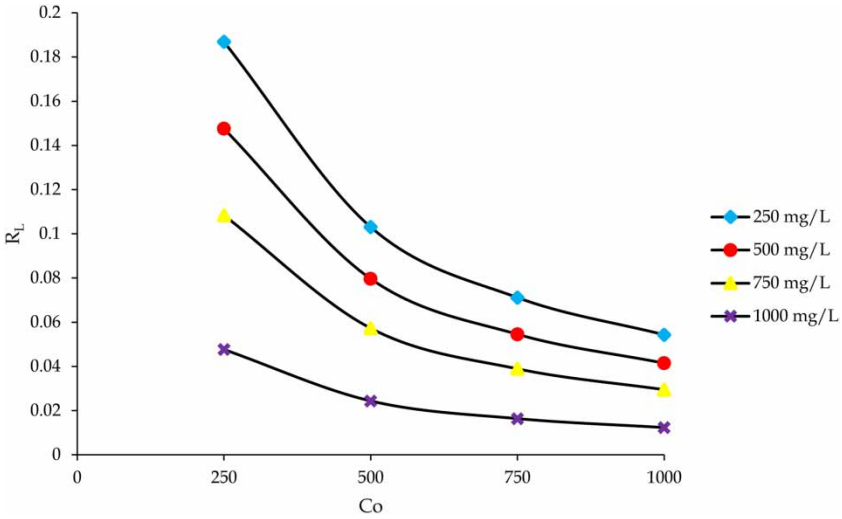

Figure 14 | Separation factor for the adsorption of calcium hardness by nZGO at room temperature.

In order to check the interference of other cations and anions in the adsorption process, an open well water sample was collected from the university campus and treated with the nZGO composite. The physiochemical parameters of well water sample are shown in Table 4. Physiochemical parameter such as pH, electric conductivity, calcium and Magnesium hardness, sulphate and nitrate, were determined with the standard methods. The synthesized nZGO (250 mg/L) was introduced in a 100 ml well water sample and stirred for 120 minutes. The results of adsorption can be seen in Table 4; the calcium ion concentration of the well water sample is reduced by 73.33%; this value is obviously less than the adsorption of calcium from the standard solution used in the study. The interference of the Mg^{++} on the adsorption can be seen clearly.

This is also a favourable one, as the magnesium ions are also a hardness contributor. The 73% of calcium hardness, along with 67% of the magnesium from the open well water sample, are removed. Apart from both cations; that is, Ca^{++} and Mg^{++}, the anions; that is, nitrate, is reduced by 45% while sulphate is reduced by 54%; on a cumulative scale, the adsorption capacity of the composite is more than the q_{max}; that is, 217 mg/g. The adsorption process for the real water sample is processed at

Water Practice & Technology Vol 15 No 4
doi: 10.2166/wpt.2020.079

Table 4 | Physicochemical parameter of open well water sample

Parameter	Before	After	% Removal
pH	7.2	7.1	–
E. Conductivity (S/m)	1,220	246	79.83
Calcium (mg/L)	120	32	73.33
Magnesium (mg/L)	230	75	67.39
Nitrate (mg/L)	21.35	11.60	45.66
Sulphate (mg/L)	62.17	28.03	54.91

neutral pH. Though the cationic adsorption on the graphene is favourable at lower pH conditions, in this composite the presence of zeolite molecular sieves governs the adsorption at neutral conditions.

Adsorption mechanism

The nZGO composite was synthesized and explored for a possible application for hardness removal. The increased surface area and structural diversity of the synthesized material have demonstrated good adsorption capacity. The possible ion exchange process of the nZGO with the Ca^{++} ions is illustrated in the following Figure 15.

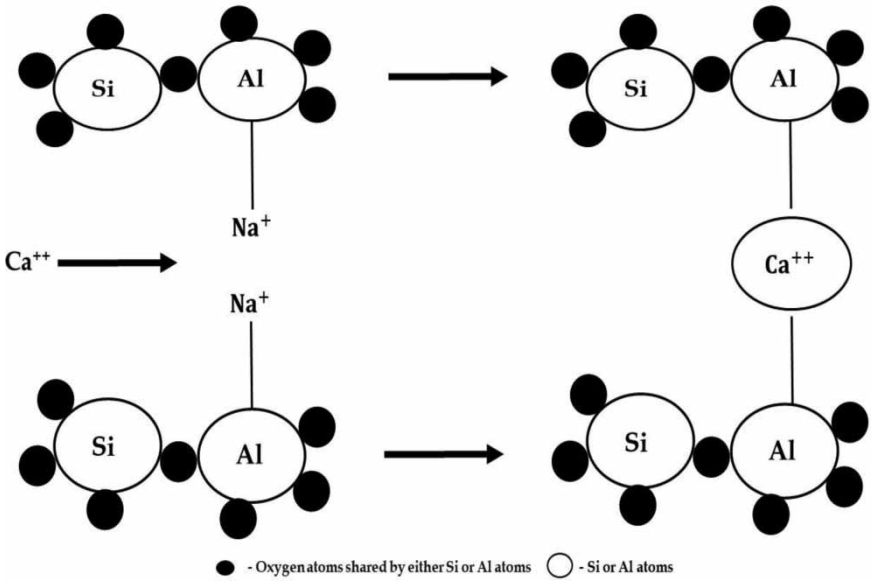

Figure 15 | Proposed ion exchange process in nZGO composites.

Zeolites normally attract cations by interfacing with the adjacent medium due to their ion-exchange properties. The heavy metal cations like rubidium, caesium, silver, cadmium, lead, zinc, barium, strontium, copper, mercury, cobalt and chromium have a great affinity for ion exchange on the zeolite surface. However, their selectivity by the zeolite framework strongly depends on the hydrated molecular size of the cations, zero point charge of the adsorbent surface and pH of the medium associated with the process. The physicochemical properties; that is, the porosity and oxygen-containing functional groups, have considerable influence on the adsorption of cations. The porous structures of the composite with a large surface area provides favourable diffusion energy levels. The adsorption performance of the native components of the composite; that is, GO and nZ, is not very satisfactory in comparison with the composite (nZGO). This is due to escalated surface interaction provided by

Water Practice & Technology Vol 15 No 4
doi: 10.2166/wpt.2020.079

the functional groups of GO in the composite with the molecular sieve of the nanozeolite. The study strongly advocates the application of nZGO composite as a promising alternative to the adsorbent materials currently available in the field of water softening treatment.

Table 5 compares various natural and commercial adsorbents' capacity for calcium hardness removal. Among all of the absorbents, the nZGO synthesized in the present study has shown maximum calcium ions removal capacity and the Q_{max} is 980 mg/L.

Table 5 | Comparison of nZGO with other adsorbents for calcium hardness removal

Adsorbent	Time	pH	Adsorbent dose	Qmax (mg/L)	Reference
Coconut shell activated carbons (CSAC)	10 h	6.3	240 g/L	655	Rolence *et al.* (2014)
Natural zeolite	30 m	6.9	50 g/L	100	Hailu *et al.* (2019)
Amberlite 748	8 h	9.5	120 mg/L	465.16	Yu *et al.* (2009)
Kaolinite smectile	30 m	8	2 g/L	100	Sheneshen *et al.* (2018)
Moringa oleifera (Seed pod husk)	40 m	7	0.3 g/L	568.4	Khati (2018)
Amorphophallus Campansulates	–	7	1.5 g/L	100	Lestari *et al.* (2018)
Coconut shell powder	3 h	7	8 g/L	557	Tomar & Rastogi (2018)
Neem leaves	3 h	7	2 g/L	500	Tomar & Rastogi (2018)
Chitosan	1 h	7	2.5 g/L	521.64	Kumar & Vishishtta (2018)
Commercial zeolite	1 h	7	6 g/L	600	Goud *et al.* (2015)
Natural pumice	6 h	–	6 g/L	57.27	Sepehr *et al.* (2013)
Modified pumice	3 h	6	6 g/L	62.34	Sepehr *et al.* (2013)
Carbon nanotube sheets	–	–	–	600	Tofighy & Mohammadi (2013)
Combined electrochemical system	–	7	–	290	Zhi & Zhang (2014)
Ion exchange resin	1 h	2–5	–	490	Gulten (2019)
nZGO	2 h	7	1 g/L	980	Present work

CONCLUSION

The nZGO nanocomposite was synthesized and successfully demonstrated its efficient adsorption potential for calcium hardness. More than 98% of calcium ions were adsorbed from 250 mg/L synthetic solution, at 120 min equilibrium time and 250 mg/L adsorbent dose. The maximum adsorption was observed at neutral pH. The removal efficiency increased with increasing adsorbent concentration. The adsorption study indicated the adsorption of calcium hardness was by the Langmuir and Temkin models, which indicates monolayer adsorption. The kinetic equilibrium data showed that the adsorption process follows pseudo-second-order kinetics and shows the adsorption process is through chemisorption. The intraparticle diffusion model indicated that it is a multi-step adsorption process. The removal of hardness from a real water sample by nZGO is also greater, it is also a good adsorbent for removing other contaminants from water. It is shown that nZGO has the best performance as an adsorbent to remove calcium hardness compared to other composites. In the view of the above, nZGO composite could be used as an effective and economical adsorbent with good practical value in the future for industrial applications.

ACKNOWLEDGEMENTS

One of the authors, Mr Ram A. Konale, sincerely acknowledges the financial support provided under DST INSPIRE Fellowship for Research Students, Scheme by Department of Science and Technology, Government of India. Grant number: DST/INSPIRE Fellowship/[IF170674].

Water Practice & Technology Vol 15 No 4
doi: 10.2166/wpt.2020.079

DATA AVAILABILITY STATEMENT

All relevant data are available from an online repository or repositories at https://drive.google.com/drive/folders/1fIJLjhk2KfQ8QSwDzlx06o1xY9KvAwiL?usp=sharing.

REFERENCES

Agarwal, S. & Rani, A. 2018 Adsorption of tannic acid from aqueous solution onto chitosan/NaOH/fly ash composites: equilibrium, kinetics, thermodynamics and modeling. *Journal of Environmental Chemical Engineering* **6**, 1486–1466.

Ahamad, M. I., Song, J., Sun, J., Wang, X., Mehmood, M. S., Sajid, M., Su, P. & Khan, A. J. 2020 Contamination level, ecological risk, and source identification of heavy metals in the hyporheic zone of the Weihe River, China. *International Journal of Environmental Research and Public Health* **17**, 1070.

Amarasooriya, A. & Kawakami, T. 2019 Removal of fluoride, hardness and alkalinity from groundwater by electrolysis. *Groundwater for Sustanable Development* **9**, 100231.

Araghia, S. H. & Entezari, M. H. 2015 Amino-functionalized silica magnetite nanoparticles for the simultaneous removal of pollutants from aqueous solution. *Applied Surface Science* **333**, 68–77.

Barathi, M., Santhana, K. K., Chinta, U. K. & Rajesh, N. 2014 Graphene oxide–aluminium oxyhydroxide interaction and its application for the effective adsorption of fluoride. *RSC Advances* **4**, 53711–53721.

Chen, J. & Lu, X. 2018 Equilibrium and kinetics studies of Cd(II) sorption on zeolite NaX synthesized from coal gangue. *Water Reuse and Desalination* **8**, 94–101.

Fegade, U., Jethave, G., Su, K. Y., Huang, W. R. & Wu, R. J. 2018 An multifunction $Zn_{0.3}mn_{0.4}O_4$ nanospheres for carbon dioxide reduction to methane via photocatalysis and reused after five cycles for phosphate adsorption. *Journal of Environmental Chemical Engineering* **6**, 1918–1925.

Ferrarini, S. F., Cardoso, A. M., Paprocki, A. & Pires, M. 2016 Integrated synthesis of zeolites using coal fly ash: element distribution in the products, washing waters and effluent. *Journal of the Brazilian Chemical Society* **27**, 2034–2045.

Gao, W., Majumdar, M., Alemany, L. B., Nrayanan, T. N., Ibarra, M. A., Pradhan, B. K. & Ajayan, P. M. 2011 Engineered graphite oxide materials for application in water purification. *ACS Applied Materials and Interfaces* **6**, 1821–1826.

Gebhardt, P., Pattinson, S. W., Ren, Z., Cooke, D. J., Elliott, J. A. & Eder, D. 2014 Crystal engineering of zeolites with graphene. *Nanoscale* **6**, 7319–7324.

Geethamani, C. K., Ramesh, S. T., Gandhimathi, R. & Nidheesh, P. V. 2013 Alkali-treated fly ash for the removal of fluoride from aqueous solutions. *Desalination and Water Treatment* **53**, 3466–3476.

Geim, A. K. & Novoselov, K. S. 2014 The rise of graphene. *Manchester Centre for Mesoscience and Nanotechnology*. https://arxiv.org/ftp/cond-mat/papers/0702/0702595.pdf

Ghaedi, M., Hajati, S., Zaree, M., Shajaripour, Y., Asfaram, A. & Purkait, M. K. 2015 Removal of methyl orange by multiwall carbon nanotube accelerated by ultrasound devise: optimized experimental design. *Advanced Powder Technology* **26**, 1087–1093.

Goud, R. V., Kumar, B. L., Abhilash, N. & Rajendra, P. P. 2015 Comparision studies on adsorbants for removal of hardness from water by using newly prepared zeolite. *International Journal Of Advances In Pharmacy, Biology And Chemistry* **4**, 342–354.

Gougazeh, M. & Buhl, J. 2013 Synthesis and characterization of zeolite A by hydrothermal transformation of natural Jordanian kaolin. *Arab Journal of Basic and Applied Sciences* **15**, 35–42.

Gulten, C. 2019 Removal of hardness of earth alkaline metals from aqueous solutions by ion exchange method. *Analytical Chemistry* **2014**, 3–7.

Hailu, Y., Tilahun, E., Brhane, A., Resky, H. & Sahu, O. 2019 Ion exchanges process for calcium, magnesium and total hardness from ground water with natural zeolite. *Groundwater for Sustainable Development* **8**, 457–467.

He, K., Chen, Y. & Zhenghua, H. Y. 2016 Removal of heavy metal ions from aqueous solution by zeolite synthesized from fly ash. *Environmental Science and Pollution Research* **3**, 2778–2788.

Hong, J. L., Maneerung, T., Koh, S. N., Kawi, S. & Wang, C. 2017 Conversion of coal fly ash into zeolite materials: synthesis and characterizations, process design, and its cost-benefit analysis. *Industrial and Engineering Chemistry Research* **56**, 11565–11574.

Izidoro, J. C., Fungaro, D. A., Abbott, J. E. & Wang, S. 2013 Synthesis of zeolites X and A from fly ashes for cadmium and zinc removal from aqueous solutions in single and binary ion systems. *Fuel* **103**, 827–834.

Jayarathna, L., Bandara, A., Ng, W. J. & Weerasooriya, R. 2015 Fluoride adsorption on $\gamma - Fe_2O_3$ nanoparticles. *Journal of Environmental Health Science and Engineering* **13**, 54.

Jethave, G., Fegade, U., Attarde, S. & Ingle, S. 2017 Facile synthesis of lead doped zinc-aluminum oxide nanoparticles (LD-ZAO-NPs) for efficient adsorption of anionic dye: kinetic, isotherm and thermodynamic behaviors. *Journal of Industrial and Engineering Chemistry* **53**, 294–306.

Jha, B. & Singh, D. N. 2018 *Fly Ash Zeolites Innovations, Applications and Direction*. Springer, Singapore. doi: 10.1007/978-981-10-1404-8.

Water Practice & Technology Vol 15 No 4
doi: 10.2166/wpt.2020.079

Kadir, N. N. & Ismail, S. 2017 Formulation study for softening of hard water using surfactant modified bentonite adsorbent coating. *Applied Clay Science* **137**, 168–175.

Kar, P., Sardar, S., Liu, B., Sreemany, M., Lemmens, P., Ghosh, S. & Pal, S. 2016 Facile synthesis of reduced graphene oxide–gold nanohybrid for potential use in industrial waste-water treatment. *Science and Technology of Advanced Materials* **17**, 375–386.

Khati, V. V. 2018 Adsorption studies on water hardness removal by using moringa oleifera seed pod husk activated carbon as an adsorbent. *International Journal of Life Sciences* **A12**, 1–8.

Kogure, T., Miyawaki, R. & Banno, Y. 2005 The true structure of wonesite, an interlayer-deficient trioctahedral sodium mica. *American Minerologist* **90**(4), 725–731.

Koshy, N. & Singh, D. 2016 Fly ash zeolites for water treatment applications. *Journal of Environmental Chemical Engineering* **4**, 1460–1472.

Kumar, M. & Vishishtta, N. 2018 Removal of nitrate and hardness from synthetic water using chitosan as an adsorbent. *International Journal of Engineering Technology Science and Research* **3**, 485–495.

Langmuir, L. 1918 The adsorption of gases on plane surfaces of glass, mica and platinum. *Journal of the American Chemical Society* **40**, 1361–1403.

Lestari, A., Malik, A., Sukirman, S., Ilmi, M. I. & Sidiq, M. 2018 Removal of calcium and magnesium ions from hard water using modified Amorphophallus campanulatus skin as a low cost adsorbent. *MATEC Web of Conference* **154**, 4–7.

Liu, L., Singh R, C. P., Webley, P. A. & Zhai, Y. 2011 Zeolite synthesis from waste fly ash and its application in CO_2 capture from flue gas streams. *Adsorption* **17**, 795–800.

Liu, D., Fang, L. & Cheng, F. 2016 Bisurfactant-assisted preparation of amorphous silica from fly ash. *Asia-Pacific Journal of Chemical Engineering*, **11**, 884–892.

Maab, N., Shokufar, A. & Ahmadi, S. 2016 The effect of temperature and type of peroxide on graphene synthesized by improved Hummers' method. *International Nano Letters* **6**, 211–214.

Madarasz, D., Szenti, I., Sapi, A., Halasz, J., Kukovecz, A. & Konya, Z. 2014 Exploiting the ion-exchange ability of titanate nanotubes in a model water softening process. *Chemical Physics Letters* **591**, 161–165.

Marcano, D. C., Kosynkin, D. V., Berlin, J. M., Sinitskii, A., Sun, Z., Slesarev, A., Alemany, J. L., Lu, W. & Tour, J. M. 2010 Improved synthesis of Graphene oxide. *ACS Nano* **4**, 4806–4814.

MeiJiao, L., Jing, L., XuYu, Y., Changan, Z., Jia, Y., Hao, H. & XianBao, W. 2013 Applications of graphene-based materials in environmental protection and detection. *Chinese Science Bulletin* **58**, 2698–2710.

Molina, A. & Poole, C. 2004 A comparative study using two methods to produce zeolites from fly ash. *Minerals Engineering* **2**, 167–173.

Mondal, N. K., Bhaumik, R. & Datta, J. K. 2016 Fluoride adsorption by calcium carbonate, activated alumina and activated sugarcane ash. *Environmental Process* **3**, 195–216.

Mozgawa, W. 2001 The realation between structure and vibrational spectra of natural zeolites. *Journal of Molecular Structure* **596**, 129–137.

Nigri, M. E., Cechinel, M. A., Mayer, D. A., Mazur, L. P., Loureiro, J. M., Rocha, S. D. & Vilar, V. P. 2017 Cow bones char as a green sorbent for fluorides removal from aqueous solutions: batch and fixed-bed studies. *Environmental Science and Pollution Research* **24**, 2364–2380.

Petriciolet, A. B., Castillo, D. M. & Avila, A. E. 2017 *Adsorption Processes for Water Treatment and Purification*. Springer, Cham, Switzerland. doi:10.1007/978-3-319-58136-1.

Rolence, C. 2016 Adsorption studies on water hardness removal by using adsorption studies on water hardness removal by using cashewnut shell activated carbon as an adsorbent. *African Journal of Science and Research* **4**, 78–81.

Rolence, C., Machunda, R. L. & Njau, K. N. 2014 Water hardness removal by coconut shell activated carbon. *International Journal of Science, Technology and Society* **5**, 97–102.

Senusi, F. & Karim, K. A. 2011 Biosorption of Pb (II) ions using rubber seed coat: equilibrium and kinetic studies. *Colloquium on Humanities, Science and Engineering Research*. Penang, Malaysia, Dec 5-6. doi:10.1109/CHUSER.2011.6163755.

Sepehr, M. N., Arrabi, M. Z., Kazemian, H., Amrane, A., Yaghmaian, K. & Ghaffari, H. R. 2013 Removal of hardness agents, calcium and magnesium, by natural and alkaline modified pumice stones in single and binary systems. *Applied Surface Sciences* **274**, 295–305.

Sheneshen, E. S., Fathy, M., Nagger, I. M., Ahmed, S. A., Shehata, N. & Shehata, A. M. 2018 Effective solutions of hardness by using adsorption technique on kaolinite smectite adsorbent from aqueous solution. *International Journal of Chemical Sciences* **16**(1), 235.

Singh, P. K. & George, S. 2018 Studies on performance characteristics of calcium and magnesium amended alumina for defluoridation of drinking water. *Journal of Environmental Chemical Engineering* **6**, 1364–1377.

Soltani, T. & Lee, B. 2016 A benign ultrasonic route to reduced graphene oxide from pristine graphite. *Journal of Colloid Interface Science* **486**, 337–343.

Soni, R. & Shukla, D. P. 2018 Synthesis of fly ash based zeolite-reduced graphene oxide composite and its evaluation as an adsorbent for arsenic removal. *Chemosphere* **219**, 504–509.

Tofighy, M. A. & Mohammadi, T. 2013 Permanent hard water softening using carbon nanotube sheets. *Desalination* **268**, 208–2013.

Tomar, Y. S. & Rastogi, D. 2018 Removal of chloride, hardness & TDS from water using different adsorbents. *International Journal for Research in Applied Science & Engineering Technology* **6**, 5111–5117.

Water Practice & Technology Vol 15 No 4
doi: 10.2166/wpt.2020.079

Weber, W. J. & Morris, J. C. 1963 Kinetics of adsorption on carbon from solution. *Journal of the Sanitary Engineering Division* **89**, 31–60.

Xia, M. & Gerson, A. R. 2018 Cr(III) removal from simulated solution using hydrous magnesium oxide coated fly ash: optimization by response surface methodology (RSM). *Chinese Journal of Chemical Engineering* **26**, 1192–1199.

Yu, Z., Qi, T., Qu, J., Wang, L. & Chu, J. 2009 Removal of Ca(II) and Mg(II) from potassium chromate solution on amberlite IRC 748 synthetic resin by ion exchange. *Journal of Hazardoues Materials* **167**(1–3), 406–412.

Zamani, S. & Tabrizi, S. N. 2016 Removal of methylene blue from water by graphene oxide aerogel: thermodynamic, kinetic, and equilibrium modeling. *Research on Chemical Intermediates* **41**, 7945–7963.

Zhang, M., Zhang, H., Xu, D., Han, L., Niu, D., Tian, B., Zhang, J., Zhang, L. & Wu, W. 2011 Removal of ammonium from aqueous solutions using zeolite synthesized from fly ash by a fusion method. *Desalination* **271**, 111–121.

Zhao, B., Sun, X., Wang, L., Zhao, L., Zhang, Z. & Li, J. 2018 Adsorption of methyl orange from aqueous solution by composite magnetic microspheres of chitosan and quaternary ammonium chitosan derivative. *Chinese Journal of Chemical Engineering* **27**, 1973–1980.

Zhi, S. & Zhang, S. 2014 A novel combined electrochemical system for hardness removal. *Desalination* **349**, 68–72.